ENG Signal Classification via Parallel Spiking Neurons for Implantable Devices

Arek Berç Gökdağ*, Silvia Mura*, Umberto Spagnolini* and Maurizio Magarini*
*Dipartimento di Elettronica, Informazione e Bioingegneria (DEIB),
Politecnico di Milano, 20133 Milano, Italy
{arekberc.gokdag, silvia.mura, umberto.spagnolini, maurizio.magarini}@polimi.it

GLOBECOM 2025 - 2025 IEEE Global Communications Conference | 979-8-3315-7781-0/25/$31.00 ©2025 IEEE | DOI: 10.1109/GLOBECOM59602.2025.11431807

***Abstract*—Neural Decoding and Stimulation (ND&S) systems offer a promising alternative to conventional treatments for peripheral nerve injuries by decoding neural signals and delivering targeted stimulation via implantable devices. A primary challenge in ND&S development is the accurate classification of electroneurography (ENG) signals under strict constraints on computational resources, processing time and power constraints. To address this, we propose a Parallel Spiking Neural Network (PSNN) architecture based on a novel spiking neuron model called Parallel Spiking Neurons (PSNs), optimized for ENG classification. The model combines event-driven processing with low computational complexity, making it well-suited for implantable applications. Compared to the state-of-the-art ESCAPE-Net, the PSNN achieves higher test accuracy (87.21%±4.9%) and macro F1-score (84.98%±9.39%), while reducing the number of the required model parameters by 99.97%. These results underscore the effectiveness of PSNNs in achieving high classification accuracy with minimal computational overhead, aligning with the stringent requirements of ND&S systems.**

I. Introduction

The Peripheral Nervous System (PNS) functions as a vital communication conduit between the Central Nervous System (CNS) and peripheral tissues, facilitating the bidirectional transmission of afferent and efferent signals essential for both voluntary motor control and involuntary physiological processes. Mechanical injury to the PNS can significantly compromise this communication pathway, leading to a wide range of clinical outcomes, including sensory disturbances, motor dysfunction, partial or complete paralysis, and the onset of chronic neuropathic pain [1].

Despite significant advances in microsurgical techniques and rehabilitative interventions, conventional treatments for peripheral nerve injuries frequently fail to achieve complete functional restoration [2]. In response to these limitations, Neural Decoding and Stimulation (ND&S) technologies have garnered increasing attention as novel therapeutic strategies. By establishing a direct interface with peripheral nerves, ND&S systems are designed to decode endogenous neural signals and deliver precisely targeted stimulation, thereby facilitating functional recovery [3].

Central to ND&S systems is the Peripheral Nerve Interface (PNI), which facilitates both the recording and stimulation of neural activity via electroneurography (ENG). ENG signals, predominantly comprising compound action potentials (CAPs) that reflect the synchronized firing of multiple nerve fibers, serve as the primary input for subsequent processing and classification processes within the ND&S framework. Building upon this neural substrate, ND&S technologies are typically structured around four core stages [3]: signal acquisition, transmission, stimuli classification, and stimulation, as detailed in Fig. 1. Accurate classification of ENG signals is essential for the functional efficacy of ND&S systems, as these systems depend on correctly identifying the neural activity stimuli to deliver precise and targeted stimulation. While substantial research has been devoted to the classification of electroencephalography (EEG) and electromyography (EMG) signals [4], [5], the classification of ENG signals remains relatively underexplored.

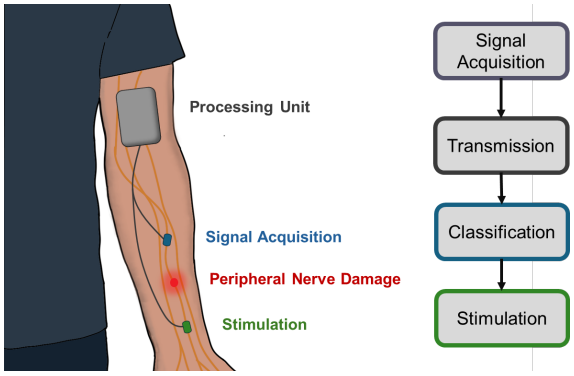

Fig. 1: Schematic representation of the ND&S system

To support implantable real-time applications, classification algorithms employed in ND&S systems must meet stringent requirements in terms of latency, accuracy, and power efficiency. In particular, these systems must be capable of generating synthetic stimulation within 300 ms to ensure real-time responsiveness, while simultaneously maintaining low power consumption to enable long-term, autonomous operation [6].

Traditional machine learning (ML) approaches, such as support vector machines (SVMs) [7], have demonstrated satisfactory performance under controlled, low-complexity conditions; however, their robustness often deteriorates in the presence of noise and variability typical of real-world environments.

Deep learning (DL) methodologies, such as artificial neural networks (ANNs), convolutional neural networks (CNNs), and long short-term memory (LSTM) networks, have shown

strong capability in modeling the nonlinear dynamics of bioelectrical signals. ANNs have been effective in classifying sensory stimuli [8], while CNNs excels at capturing spatial and temporal features from high-density multi-contact cuff electrodes [3]. ConvLSTM models further improve performance on longer sequences by modeling spatiotemporal dependencies [9]; however, their computational complexity limits suitability for implantable systems, where CNNs offer a more favorable trade-off between accuracy and efficiency [3]. Among CNN-based models, ESCAPE-NET [10] is a leading architecture that leverages both spatial and temporal correlations in ENG signals to achieve state-of-the-art classification. Yet, its high computational cost poses challenges for real-time, low-power and low-complexity applications, underscoring the persistent trade-offs among accuracy, energy efficiency, and system complexity [11]

Despite recent progress, existing neural stimuli classification models often fall short of the stringent requirements of ND&S systems, particularly regarding accuracy, power efficiency, and complexity. To address this challenge, this work investigates the viability of a spiking neural network (SNN) architecture based on Parallel Spiking Neurons (PSNs) [12] for ENG signal classification. This approach leverages the event-driven and temporally precise nature of SNNs, which aligns well with the sparse and time-dependent characteristics of neural signals. Furthermore, the low computational complexity of the PSN-based architecture makes it particularly suitable for low-complexity, implantable neuroprosthetic systems. Its performance, evaluated in terms of classification accuracy, F1-score, and computational complexity, is compared with the state-of-the-art ESCAPE-NET [10], illustrating the trade-offs among classification accuracy and F1-score, and computational complexity. In particular, the PSN-based model achieves 87.21% accuracy and an 84.98% F1-score, outperforming ESCAPE-NET while using only 25,463 parameters, which represents a 99.97% reduction compared to ESCAPE-NET. These findings highlight the principal advantage of the proposed PSNN: it delivers state-of-the-art accuracy with a fraction of the complexity of CNN-based methods. By combining high accuracy, robustness across subjects, and extreme computational efficiency, the PSNN emerges as a compelling candidate for real-time neural decoding in implantable ND&S systems.

Organization: The paper is organized as follows: Section II introduces the system model, while Section III details ENG signal preprocessing. Classification methods, both state-of-the-art and proposed, are presented in Section IV. Numerical results are reported in Section V, and conclusions are drawn in Section VI.

Notation: Lower-case letters $\mathbf{x}$ refer to vectors and the notation x_k refers to the kth element, upper-case bold letters $\mathbf{X}$ refers to matrices . The symbols $||\cdot||$, $\mathbb{E}$ and $\mathbb{R}$ refer to the Euclidean norm operator, expectation operator, and to the real number set, respectively. While $\mathcal{X}$ refers to a set.

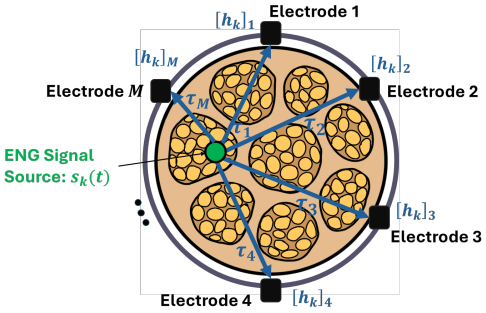

Fig. 2: System model illustration of a single ring from a multi-ring cuff electrode, showing ENG source $s_k(t)$ propagating to electrodes with delay τ_l and volume-conducted propagation $[h_k]_l$.

II. System Model

Peripheral nerves are composed of hierarchically organized fascicles that bundle densely packed axons, enabling the bidirectional propagation of ENG signals. Afferent axons transmit sensory information from peripheral receptors to the CNS, while efferent axons carry motor commands from the CNS to peripheral effectors. This continuous bidirectional flow of neural activity supports real-time integration of sensory feedback and motor execution, emphasizing the critical role of the PNS in mediating organism-environment interactions.

This neural activity is recorded using a cylindrical cuff electrode that encircles the nerve and consists of N longitudinal rings, each with M uniformly spaced contacts, resulting in $L = M \times N$ electrodes that offer extensive spatial coverage and directional sensitivity. Assuming K mutually uncorrelated neural sources, the multichannel ENG observation $\mathbf{y}(t) \in \mathbb{R}^{L\times 1}$ is modeled as

$$\mathbf{y}(t) = \sum_{k=1}^{K} \mathbf{h}_k \, s_k\big(t - \boldsymbol{\tau}_k\big) + \mathbf{w}(t), \tag{1}$$

where $\mathbf{h}_k \in \mathbb{R}^{L\times 1}$ encodes volume-conducted propagation from the k-th source to each electrode, with the lth element defined as in [3]

$$[\mathbf{h}_k]_l = -\frac{1}{4\pi\sigma\|\mathbf{p}_l - \mathbf{p}_k\|^2},$$

where σ refers to the conductivity and $\mathbf{p}_l, \mathbf{p}_k$ the electrode and source coordinate in a global reference system, respectively. The source waveform $s_k(t)$ is represented as a superposition of CAPs generated by synchronous activation of axons; afferent and efferent fibers are both admissible sources. Mutual independence of the sources is assumed for simplicity, $\mathbb{E}[s_k(t)s_{k'}(t)] = 0$ for $k \neq k'$. Transmission delays between each source and electrode are collected in $\boldsymbol{\tau}_k = [\tau_{k,1}, \ldots, \tau_{k,L}]^{\mathsf{T}}$, capturing spatio-temporal dispersion along the nerve axis.

Additive disturbance $\mathbf{w}(t)$ aggregates global interference such as EMG interference, electrode-specific artifacts, and

white Gaussian thermal noise. Crucially, these perturbations exhibit both spatial and temporal correlations, i.e., $\mathbb{E}[w_l(t)w_{l'}(t)] \neq 0$ for $l \neq l'$ and $\mathbb{E}[w_l(t)w_{l'}(t')] \neq 0$ for $t \neq t'$ across electrodes and time samples.

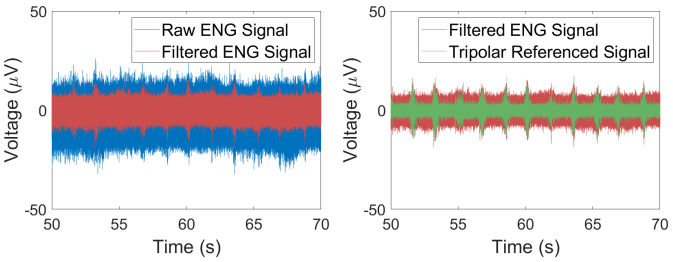

(a) (b)

Fig. 3: Preprocessing pipeline showing (a) bandpass filtering, and (b) tripolar referencing for noise reduction.

III. Signal Preprocessing and CAP Detection

This section presents the experimental dataset and preprocessing pipeline used for ENG signal classification. Recordings were collected from the sciatic nerves of nine Long Evans rats (from Rat2 to Rat10) during controlled hind limb stimulation [13]. The dataset comprises three stimulus types: dorsiflexion, plantarflexion, and pricking. Each recording session lasted approximately 180 seconds and included around 100 stimulation events per condition, manually applied in synchrony with a 70 bpm metronome to ensure standardized timing. ENG signals were acquired using a 56-channel multicontact cuff electrode, organized into seven longitudinal rings, and sampled at 30 kHz to capture fine neural dynamics.

A robust preprocessing pipeline is essential due to the inherently low signal-to-noise ratio (SNR) of ENG signals [10]. Building upon the pipeline introduced in [10], this work introduces enhancements, including segmentation, signal conditioning, and denoising. The pipeline is designed to reliably detect CAPs, characterized by synchronized, spike-like waveforms, which form the basis for subsequent neural activity classification and it is defined as

1) ***Amplitude clipping:*** Signals in (1) are first clipped within a range of $\pm 40\ \mu V$ to suppress outliers while preserving the underlying neural content.
2) ***Band-pass filtering:*** A sixth-order Butterworth filter with a passband of 800 Hz to 5 kHz is applied to attenuate low-frequency EMG interference and high-frequency impedance noise, as shown in Fig. 3a.
3) ***Tripolar referencing:*** To enhance the isolation of neural signals from background interference, the outermost rings of the cuff electrode array are utilized as reference electrodes [14]. This configuration enables the estimation and removal of common-mode components in $\mathbf{w}(t)$, as demonstrated in Fig. 3b.
4) ***Segmentation into activity intervals:*** Signals are segmented into active ($\mathcal{T}_{on}$) and inactive ($\mathcal{T}_{off}$) intervals by applying a moving mean absolute value (MMAV) to detect peaks corresponding to stimulation events, as illustrated in Fig. 4a. A 0.64-second window is extracted around each peak and assigned to $\mathcal{T}_{on}$. Although the stimulation duration is approximately 0.86 seconds based on a 70 BPM metronome, a shorter window is used to accommodate timing variability and exclude transitional periods, ensuring stable neural responses are captured.

TABLE I: SNR in dB across various rats and classes within the analyzed dataset.

#Rat	Dorsiflexion	Plantarflexion	Pricking
4	1.81	2.44	2.42
5	2.03	2.12	2.83
6	3.59	1.24	1.59
7	0.23	1.97	0.87
8	0.93	1.96	0.55
9	1.60	0.41	0.61

5) ***SNR estimation:*** The SNR is defined as the ratio between the signal power measured during $\mathcal{T}_{\text{on}}$ and the noise power measured during $\mathcal{T}_{\text{off}}$, averaged across all recording electrodes

$$\text{SNR} = \frac{1}{\xi L} \frac{\sum_{t \in \mathcal{T}_{\text{on}}} \left\| \mathbf{y}(t) \right\|^2}{\sum_{t \in \mathcal{T}_{\text{off}}} \left\| \mathbf{y}(t) \right\|^2}, \tag{2}$$

where ξ normalizes for the number of samples. Recordings exhibiting SNR values less than or equal to zero (Rat2, Rat3, and Rat10) are excluded from the analysis, while the other subjects' SNRs are shown in Table I. These exclusions ensure the reliability of subsequent classification analyses by preserving the integrity of the dataset.
6) ***CAP detection:*** CAPs are identified by detecting local peaks in the processed signal using an upper threshold $\gamma_{\text{up}} = 6 \cdot \text{std}\{\mathbf{y}(t) | t \in \mathcal{T}_{\text{on}}\}$ and a lower threshold $\gamma_{\text{low}} = (4 \cdot |\text{med}\{\mathbf{y}(t) | t \in \mathcal{T}_{\text{off}}\}|)/0.6745$ as in [10], where $\text{std}\cdot$ denotes the standard deviation $\text{med}\cdot$ denotes the median. Peaks with amplitudes between these thresholds are retained and classified as CAPs, as shown in Fig. 4b.

IV. ENG Signals Classification

This section presents the models employed to classify dorsiflexion, plantarflexion, and pricking stimuli from processed ENG recordings. Both CNNs and SNNs are evaluated, with ESCAPE-Net [10] serving as a strong CNN baseline. In contrast, the proposed SNN architecture leverages temporal coding mechanisms to enhance classification performance while substantially reducing computational demands. Achieving this balance is critical for ND&S systems, where both efficiency and accuracy are essential for practical deployment. For consistency, all models are trained and tested on the same dataset and preprocessing pipeline, as described in Sect. III.

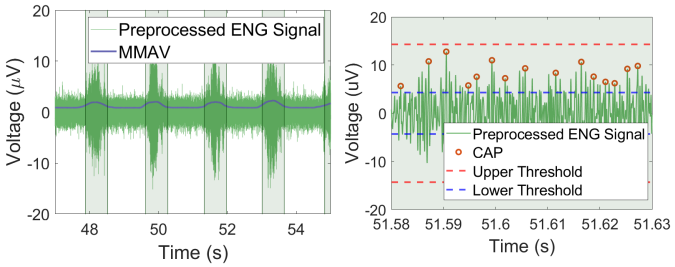

(a) (b)

Fig. 4: (a) Detection of active periods via MMAV. (b) CAP identification using amplitude-based thresholds.

A. ESCAPE-Net

ESCAPE-Net is a CNN architecture specifically designed for ENG signal classification, addressing the challenges associated with detecting complex temporal and spatial patterns [10]. The network comprises three convolutional layers with progressively smaller kernel sizes (8×8, 4×4, and 2×2), each employing 64 filters and ReLU activation to enhance feature learning. Max-pooling operations with same padding and a stride of one follow the first two convolutional layers, enabling spatial downsampling while preserving spatial dimensions. After feature extraction, the output is flattened and passed through a fully connected layer with 256 neurons. A final softmax layer with three neurons is used for multi-class classification. Through its hierarchical design, ESCAPE-Net effectively captures multi-scale features in ENG signals, achieving strong classification performance and robust generalization capabilities.

B. Parallel Spiking Neural Network

SNNs, inspired by biological neurons, encode and transmit information through discrete spikes, making them inherently suited for temporal data processing. Conventional spiking neuron models, such as the Leaky Integrate-and-Fire and Parametric Leaky Integrate-and-Fire neurons [15] rely on recursive membrane dynamics and reset mechanisms that inherently limit their computational parallelism and efficiency. The novel model, PSN [12], addresses these limitations by eliminating the membrane potential reset operation. This simplification enables a closed-form expression for the membrane potential and removes the need for step-by-step iteration [12]. Specifically, its evolution can be described as:

$$V(t) = \left(1 - \frac{1}{\rho}\right) V(t-1) + \frac{1}{\rho} X(t), \tag{3}$$

where $X(t)$ denotes the input current at time step t, and ρ is the membrane time constant. Due to the linearity of this update, the membrane potential at any time step can be rewritten as a weighted sum over past inputs [12]:

$$V(t) = \sum_{i=0}^{T-1} W_{t,i} \cdot X(i), \tag{4}$$

which, over all time steps, yields the matrix–vector formulation $\mathbf{v} = \mathbf{W}\mathbf{x}$, where $\mathbf{x} \in \mathbb{R}^{T\times 1}$ is the input signal, $\mathbf{v} \in \mathbb{R}^{T\times 1}$ the membrane potential vector, and $\mathbf{W} \in \mathbb{R}^{T\times T}$ a weight matrix that defines the neuron's temporal dynamics. In the PSN model, $\mathbf{W}$ is treated as a learnable parameter, which marks a core difference [12]: unlike traditional spiking neurons, where such weights are fixed by decay dynamics, PSNs allow these temporal dependencies to be optimized during training. This flexibility enables each potential v_t to adaptively integrate information from the entire input sequence, making the PSN particularly suited for modeling longer temporal patterns.

Finally, the output spike train $\mathbf{s} \in \{0,1\}^{T\times 1}$ is generated by applying a thresholding function:

$$\mathbf{s} = \Theta\left(\mathbf{W}\mathbf{x} - \mathbf{v}^{\text{th}}\right), \tag{5}$$

where $\mathbf{v}^{\text{th}} \in \mathbb{R}^{T\times 1}$ is a trainable threshold vector, and $\Theta(\cdot)$ is the element-wise Heaviside step function [12].

By reformulating the membrane potential computation as a matrix–vector operation, PSNs enable parallel evaluation across all time steps, which significantly accelerates simulation and improves scalability. Moreover, the learnable temporal kernel $\mathbf{W}$ enhances the network's ability to model long-term dependencies in sequential data, making PSNs a promising architecture for efficient spiking-based learning.

This study introduces a PSN Network (PSNN) for classifying ENG signals. For each detected CAP, as described in Sec. III, a 100-sample window is extracted and centered on the CAP peak identified in the signal from the middle ring of the cuff electrode. This temporal reference is then used to extract aligned windows across all $L = 56$ channels, ensuring consistent spatial and temporal representation. The resulting multichannel segments are standardized using training-set statistics and input directly into the PSNN as continuous-valued signals, without spike encoding or conversion into spike trains. The intermediate layers of the PSNN consist of PSNs that transform the input spatiotemporal patterns into a higher-level representation suitable for classification. At the output, three non-spiking neurons compute the temporal average of their inputs and apply a softmax function to produce class membership probabilities, effectively capturing the dynamics of the signal in a stable and interpretable form.

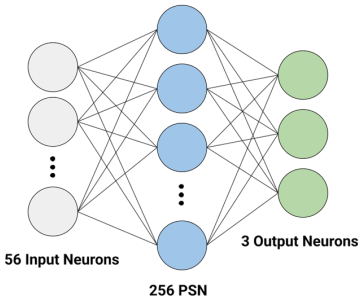

Fig. 5: Architecture of the proposed PSNN model

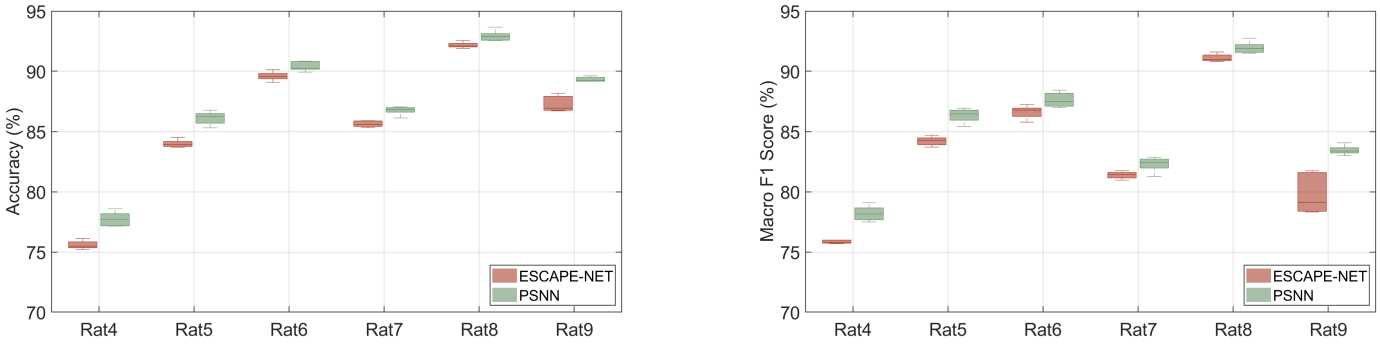

Fig. 6: Comparison of classification performance between ESCAPE-NET and PSNN across different rats (Rat4 to Rat9). (a) Accuracy (%) , (b) Macro F1 score

The proposed PSNN architecture consists of a single hidden layer comprising 256 PSNs, selected to balance classification performance with computational efficiency. This configuration is identified through a systematic grid search employing a hold-out validation strategy designed to minimize computational overhead. The dataset is partitioned using a stratified random split into 65% training, 20% validation, and 15% testing subsets. The test set remained isolated throughout the search and is reserved for final model evaluation described in Sect. V. The search space includes 12 candidate architectures, encompassing both single- and two-layer configurations, with each layer containing 56, 128, or 256 neurons. The search spaces are selected based on preliminary evaluations showing they effectively capture the underlying structure of ENG signals for accurate classification.

The evaluation is conducted using datasets from Rat 4, 5, and 6, chosen for their high SNRs to ensure reliable assessment under favorable conditions. Grid search optimization targeted three metrics: classification accuracy, macro-averaged F1 score, and total trainable parameters. Accuracy measures the proportion of correct predictions across all samples. The F1 score, the harmonic mean of precision and recall, balances false positives and false negatives. The macro-averaged F1 score extends this by averaging F1 scores across classes, giving equal weight to each and mitigating the effects of class imbalance.

Among the evaluated configurations, the single-layer architecture with 256 PSN neurons yields the most favorable trade-off between performance and computational complexity, achieving an average validation accuracy of 85.51% and a macro F1 score of 84.7%. Although alternative two-layer configurations, such as [256, 56], [256, 128], and [256, 256] achieved slightly higher scores (Table II), their improvements were negligible relative to the substantial increase in parameters. As a result, the single-layer [256] configuration (Fig. 5) is selected for the final PSNN model. This selection leads to a parameter reduction of approximately 75% compared to the most complex candidate.

TABLE II: Validation results for top configurations of grid search, averaged across Rat4, Rat5, and Rat6.

Model	Accuracy (%)	Macro F1 Score (%)	Total Parameters
[256]	85.91	85.30	25463
[256, 56]	85.96	85.77	49355
[256, 128]	86.15	85.73	68075
[256, 256]	86.15	85.58	101355

V. Numerical Results

This section presents the experimental results for the classification of ENG stimuli using the proposed SNN architecture, PSNN with ESCAPE-Net [10] serving as a CNN baseline.

To ensure robust and generalizable results, the dataset is partitioned, using the previously separated independent test set, while the remaining 85% is used for training and validation with 5-fold cross-validation, each fold selected in a stratified randomized way. This strategy enables performance metrics to capture variability across different data splits, reduces the risk of overfitting, and ensures an unbiased final evaluation. For this results all the subjects (Rat 4-9) are used.

Models are assessed using classification accuracy, F1 score, macro-averaged F1 score, and total trainable parameters (as defined in Sec. IV), providing a comprehensive evaluation of predictive performance and model complexity.

A subject-wise evaluation, as illustrated in Fig. 6a and Fig. 6b, highlights the consistency of the PSNN's performance across different subjects. Across these subjects, PSNN consistently outperforms ESCAPE-Net. In terms of macro F1-score, PSNN achieves values of 82.28%, 91.95%, and 83.45% for Rat 7, 8, and 9, respectively, compared to 81.38%, 91.12%, and 79.83% for ESCAPE-Net. Similarly, classification accuracies of 86.74%, 92.93%, and 89.33% are observed for PSNN, surpassing ESCAPE-Net's corresponding values of 85.63%, 92.17%, and 87.29%. These outcomes reinforce the robustness of the PSNN approach across diverse recording conditions, affirming its effectiveness in ENG signal classification.

Building upon this evaluation framework, the results shown in Tab. III demonstrate clear performance advantages of the proposed PSNN model. Specifically, PSNN achieves a mean

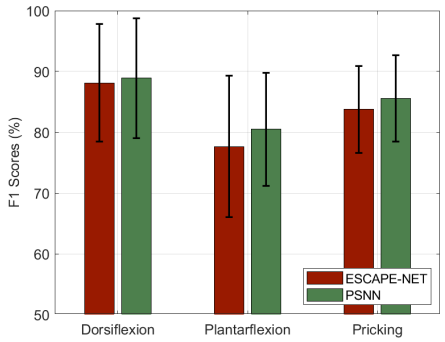

Fig. 7: Comparison of F1 scores for different stimulation types. Bars represent mean F1 scores with error bars indicating standard deviation.

test accuracy of 87.21% ±4.9%, surpassing ESCAPE-Net's 85.71%±5.34% by 1.50 percentage points. Likewise, PSNN attains a higher macro F1-score of 84.98%±9.39%, compared to 83.18%±10.49% for ESCAPE-Net, reflecting an improvement of approximately 1.8 in F1-score. While the mean gains may appear modest, the consistently lower standard deviation exhibited by PSNN suggests greater stability and generalization across subjects. These findings underscore the enhanced classification reliability and efficiency of the PSNN architecture in the context of ENG signal classification.

Further insights are provided by the class-wise F1-score analysis. As depicted in Fig. 7, PSNN achieves F1-scores of 89% for dorsiflexion, 80% for plantarflexion, and 85% for pricking, whereas ESCAPE-Net attains scores of 88%, 78%, and 84% respectively. Although plantarflexion remains the most challenging class for both models, PSNN consistently delivers superior classification across all categories, reinforcing its enhanced ability to distinguish between neural activity patterns.

Beyond its performance advantages, the PSNN architecture demonstrates a substantial reduction in model complexity. While ESCAPE-Net requires approximately 91.8 million trainable parameters, the PSNN model achieves comparable or superior classification performance with only 25463 parameters as shown in Table III. This represents a reduction of approximately 99.97% in parameter count. This drastic improvement in computational efficiency positions PSNN as a highly promising candidate for deployment in resource-constrained environments, including implantable neural decoding and stimulation systems. Overall, these findings confirm that PSNN achieves a favorable balance between classification performance and computational efficiency, thereby supporting its applicability in practical ND&S system applications.

TABLE III: Test results for PSNN and ESCAPE-NET.

Model	Accuracy (%)	Macro F1 Score (%)	Total Parameters
PSNN	87.21	84.98	25463
ESCAPE-NET	85.71	83.18	91837635

VI. Conclusion

This work addresses the challenge of achieving accurate ENG signal classification within the stringent computational constraints of implantable ND&S systems. To this end, we propose a PSNN architecture designed to balance classification performance with model efficiency. The proposed model achieves state-of-the-art performance, surpassing ESCAPE-Net with a test accuracy of 87.21% and a macro F1-score of 84.98%. Notably, this is accomplished with only 25463 trainable parameters, a 99.97% reduction in model complexity compared to ESCAPE-Net. These outcomes underscore the central advantage of the proposed PSNN, namely its ability to match or surpass the performance of SOTA methods while maintaining exceptional efficiency, thereby offering a practical solution for real-time neural decoding in implantable ND&S systems.

References

[1] M. L. Wang, M. Rivlin, J. G. Graham, and P. K. Beredjiklian, "Peripheral nerve injury, scarring, and recovery," *Connective Tissue Research*, Jan. 2019.

[2] G. Hussain, J. Wang, A. Rasul, H. Anwar, M. Qasim *et al.*, "Current status of therapeutic approaches against peripheral nerve injuries: A detailed story from injury to recovery," vol. 16, no. 1, pp. 116–134.

[3] A. Coviello, F. Linsalata, U. Spagnolini, and M. Magarini, "Artificial neural networks-based real-time classification of ENG signals for implanted nerve interfaces," *IEEE JSAC*, vol. 42, no. 8, pp. 2080–2095, Aug. 2024.

[4] A. Phinyomark and E. Scheme, "EMG pattern recognition in the era of big data and deep learning," *Big Data and Cognitive Computing*, vol. 2, no. 3, p. 21, Sep. 2018.

[5] G. Li, C. H. Lee, J. J. Jung, Y. C. Youn, and D. Camacho, "Deep learning for EEG data analytics: A survey," *Concurrency and Computation: Practice and Experience*, vol. 32, no. 18, p. e5199, 2020.

[6] T. R. Farrell and R. F. Weir, "The optimal controller delay for myoelectric prostheses," *IEEE TNSRE*, vol. 15, no. 1, pp. 111–118, 2007.

[7] E. Brunton, C. W. Blau, and K. Nazarpour, "Separability of neural responses to standardised mechanical stimulation of limbs," vol. 7, no. 1, p. 11138. [Online]. Available: https://www.nature.com/articles/s41598-017-11349-z

[8] R. G. L. Koh, A. I. Nachman, and J. Zariffa, "Classification of naturally evoked compound action potentials in peripheral nerve spatiotemporal recordings," vol. 9, no. 1, p. 11145.

[9] "Classification of sensory neural signals through deep learning methods."

[10] R. G. L. Koh, M. Balas, A. I. Nachman, and J. Zariffa, "Selective peripheral nerve recordings from nerve cuff electrodes using convolutional neural networks," *Journal of Neural Engineering*, vol. 17, no. 1, p. 016042, Jan. 2020.

[11] A. B. Gokdag, S. Mura, A. Coviello, M. Zhu, M. Magarini, and U. Spagnolini, "Low-complexity CNN-based classification of electroneurographic signals."

[12] W. Fang, Z. Yu, Z. Zhou, D. Chen, Y. Chen, Z. Ma, T. Masquelier, and Y. Tian, "Parallel spiking neurons with high efficiency and ability to learn long-term dependencies," in *NeurIPS*, Nov. 2023.

[13] J. Zariffa, "Replication data for: Koh, Ryan GL, Adrian I. Nachman, and José Zariffa. "Classification of naturally evoked compound action potentials in peripheral nerve spatiotemporal recordings." Scientific reports 9:11145, 2019." 2023. [Online]. Available: https://doi.org/10.5683/SP3/JRZDDR

[14] J. Struijk and M. Thomsen, "Tripolar nerve cuff recording: Stimulus artifact, EMG and the recorded nerve signal," in *IEEE EMBC*, vol. 2, Sep. 1995, pp. 1105–1106 vol.2.

[15] W. Fang, Z. Yu, Y. Chen, T. Masquelier, T. Huang, and Y. Tian, "Incorporating learnable membrane time constant to enhance learning of spiking neural networks," Aug. 2021.